



Evaluation of a forest parameterization to improve boundary layer flow simulations over complex terrain

Julian Quimbayo-Duarte¹, Johannes Wagner², Norman Wildmann², Thomas Gerz², and Juerg Schmidli¹

¹Institute for Atmospheric and Environmental Sciences, Goethe University Frankfurt, Frankfurt am Main, Germany

²Deutsches Zentrum für Luft- und Raumfahrt e.V., Institut für Physik der Atmosphäre, Oberpfaffenhofen, Germany

Correspondence: Julian Quimbayo-Duarte (quimbayo-duarte@iau.uni-frankfurt.de)

Abstract. We evaluate the influence of a forest parametrization on the simulation of the boundary layer flow over moderate complex terrain in the context of the Perdigão 2017 field campaign. The numerical simulations are performed using the Weather research and forecasting model using its large eddy simulation mode (WRF-LES). The short-term high resolution (40 m horizontal grid spacing) and long-term (200 m horizontal grid spacing) WRF-LES are evaluated for an integration time of 12 hours and 1.5 months, respectively, with and without forest parameterization. The short-term simulations focus on low-level jet events over the valley, while the long-term simulations cover the whole intensive observation period (IOP) of the field campaign. The results are validated using lidar and meteorological tower observations. The mean diurnal cycle during the IOP shows a significant improvement of the along-valley wind speed and the wind direction when using the forest parametrization. However, the drag imposed by the parametrization results in an underestimation of the cross-valley wind speed, which can be attributed to a poor representation of the land surface characteristics. The evaluation of the high-resolution WRF-LES shows a positive influence of the forest parametrization on the simulated winds in the first 500 m above the surface.

1 Introduction

In recent years the rising computational power allowed numerical weather prediction models to run with higher spatial resolutions in real case mode. The grids are now fine enough to fully resolve the atmosphere with techniques such as large eddy simulation (LES). LES makes it possible to describe the interaction of a turbulent flow with obstacles affecting the development of the boundary layer such as hills, forest-, urban canopies, etc (Dupont and Brunet, 2008). Tree clusters or urban blocks start to be in the spatial scale of numerical models, evidencing the need to improve the representation of surface characteristics (Shaw and Schumann, 1992).

Moreover, when the model vertical and horizontal resolution decrease to tens (or hundreds) of metres, the representation of the surface obstacles becomes critical (Aumond et al., 2013). The classical representation of such obstacles is normally introduced into mesoscale models using a bulk approach such as a characteristic roughness length (Z_o) in each grid cell. However, the effect of the ground obstacles should be taken into account not only through surface schemes, but also within the dynamic equations of the numerical model such as in the drag force approach (Zaïdi et al., 2013).



Several works have successfully implemented the drag force approach in LES to deal with the impact of vegetation canopies on the flow development over both flat and complex terrain. Dupont et al. (2008) implemented the drag-force approach by adding a pressure and a viscous drag term in the momentum equation to account for vegetation in the numerical domain (using the Advanced Regional Prediction System, ARPS). Results from the LES of turbulent flow within and above a forested canopy, in a controlled environment, were validated against pressure and velocity data from a wind tunnel experiment.

Mazoyer et al. (2017) used LES to simulate a radiation fog event observed during the ParisFog experiment. The model included the drag effect of a tree barrier by introducing an additional term into the momentum and turbulent kinetic energy (TKE) equations (using the Meso-NH model). The model performance was satisfactory, as it produced a reasonably good agreement with the near-surface measurements and liquid water path.

Liu et al. (2016) studied the drag effects from vegetation in airflow over real terrain. The vegetation canopy was modelled by adding a negative friction term in the momentum equation. Results from the LES showed satisfactory agreement with the experiments. The model predicted well the non-isotropic characteristics of turbulence in the wake region.

Wagner et al. (2019a) explored a set of long-term numerical simulations using a forest parametrization base on the drag-force approach. The results agree with observations, although the authors did not present model results without forest parameterization. An evaluation of model performance with/without forest parameterization is still needed to measure its impact on model performance.

In the present work, we evaluate the performance of LES with a forest canopy parametrization in the context of the Perdigão 2017 field campaign (Fernando et al., 2019). For this purpose, a configuration similar to that presented in Wagner et al. (2019a) is used with the addition of a subsequent inner domain with a horizontal resolution of 40 m. Numerical simulations with/without the forest parametrization using the Weather Forecast and Research model (WRF) version 4.0.1 (Skamarock et al., 2019) are presented. Results are validated and tested against observational data retrieved during the campaign's intensive observational period (IOP) comprised between May and June 2017. In here, we take up the work of Wagner et al. (2019b) and further explore the effect of the forest parametrization in the WRF-LES long/short term simulations.

The paper is organised as follows. A brief description of the instrumentation used to validate the model is given in section 2 along with a description of the model and the forest parametrization. The results are presented and discussed in section 3. The conclusions are drawn in section 4.

2 Materials and Methods

2.1 The Perdigão Field Campaign

The Perdigão 2017 field experiment was an international effort with the goal of studying the microscale flow over two nearly parallel mountain ridges located in central Portugal (see Fig. 1a). The campaign is part of the New European Wind Atlas (NEWA) project (Mann et al., 2017). The two mountain ridges are oriented approximately 35° from north in the counterclockwise direction separated from each other by about 1400 m. Both ridges are located at about 460 m above the ground level (AGL), while the near surrounding terrain at 260 m AGL. Based on the long-term measurements performed before the field



<i>Instrument</i>	<i>Name</i>	<i>Location</i>
100 m Met tower	T20 (tse04)	7°44'37.37"W 39°42'21.47"N
100 m Met tower	T25 (tse09)	7°44'5.40"W 39°42'40.36"N
100 m Met tower	T29 (tse13)	7°43'49.38"W 39°42'48.97"N
Scanning LIDAR	WS1	7°44'38.95"W 39°42'22.08"N
Scanning LIDAR	WS2	7°44'36.01"W 39°42'23.58"N
Scanning LIDAR	WS3	7°43'49.68"W 39°42'48.69"N
Scanning LIDAR	WS4	7°43'47.47"W 39°42'50.12"N
Scanning LIDAR	CLAMPS	7°44'13.65"W 39°42'45.35"N

Table 1. List of the instrumentation used in the present work along with its location (WSG84 coordinates). The location of each instrument is showed in Fig. 1c.

campaign, the wind direction is observed to be primary from the southwest, perpendicular to the ridge orientation. A secondary pattern, mainly occurring during the nighttime, is wind from northeast, which is also perpendicular to the ridges Fernando et al. (2019). The campaign included an intensive observation period (IOP) between 1 May and 15 June 2017.

60 A large amount of instrumentation were deployed in the area near the parallel mountain ridges. The instrumentation included meteorological towers, lidars, microwave radiometers, radiosondes, wind profilers, radio acoustic sounding systems and micro-
phones providing a unique data pool of meteorological observations in complex terrain (Fernando et al., 2019). In the present
work, we use data from the meteorological towers and the lidars to evaluate the numerical model. All the instruments used
in the present work are listed in table 2.1, and their location is shown in Fig. 1c. Further information on all instrumentation
65 available during the field campaign can be found at the campaign's official web-page <https://perdigao.fe.up.pt/> (re3data.org, 2019).

Data from the 100 m meteorological towers along the southeast transect (TSE; equal to transect 2 in Fernando et al. (2019)) are used to evaluate the numerical simulations with and without forest parameterization. The towers were equipped with sonic anemometers at 20, 40 ,60, 80 and 100m AGL.

70 Four of the wind scanners (WS1 to WS4) were performing range-height indicator (RHI) scans across the double ridge parallel to a wind direction of 234.68°, which defines TSE. The scanning strategy was such that WS1 and WS3 were scanning towards the southwest using an azimuth angle of 234.68°, while WS2 and WS4 were scanning towards the northeast with an azimuth angle of 54.68°. Note that WS2 and WS4 are not shown in Fig. 1c, as they are located close to WS1 and WS3 respectively. The combination of the four lidars enables to produce lidar composites of radial velocities perpendicular to the
75 double ridge (Menke et al., 2019). The latter is called "cross-valley" direction, and the direction parallel to the double-ridge is called "along-valley" in the present study.

The University of Oklahoma deployed a Halo Photonics Stream Line scanning lidar as part of the Collaborative Lower Atmospheric Mobile Profiling System (CLAMPS, see Wagner et al. (2019c)). The instrument was set to different scanning



scenarios, but in the present study we use the data from a regular sequence of velocity azimuth display (VAD) scans every two
80 minutes (see Fig. 1c).

2.2 Numerical simulation setup

The numerical simulations were performed using the WRF model version 4.0.1 (Skamarock et al., 2019). Two sets of LES have
been conducted, which differ from each other in the horizontal grid spacing of the innermost domain and the total integration
time. The first set consists of long term simulations ran for 49 days using the same setup as in Wagner et al. (2019a) with three
85 nested domains D01, D02 and D03 with a horizontal grid spacing of 5 km, 1 km and 200 m, respectively (see Fig. 1a and
Fig. 1b).

The second set was identical to the first, but it included a fourth nested domain D04 with a horizontal grid spacing of 40 m
(see Fig. 1c). The second set, however, has been ran for selected periods (below described). Domains d01 and d02 were run in
RANS (Reynolds Averaged Navier Stokes) mode, while domains D03 and D04 were run in LES mode. The high resolution of
90 D04 was chosen to better resolve the double ridge. As in Wagner et al. (2019a) vertical nesting was applied to define individual
levels in the vertical for each model domain. For the domains D01 to D04, 36, 57, 70 and 82 vertically stretched levels were
used and the respective lowest mass point was set at 80 m, 50 m, 15 m and 10 m AGL. The model top was set at 200 hPa (about
12 km height). In the RANS domains (D01 and D02) the Mellor-Yamada-Janjic turbulent kinetic energy (TKE) scheme was
used (Mellor and Yamada, 1982). In contrast, the simulations in Wagner et al. (2019a) used the YSU-scheme (Hong and Kim,
95 2008). The other physics parameterizations were the same as in Wagner et al. (2019a).

Initial and boundary conditions were provided by the ECMWF operational analyses on 137 model levels with a horizontal
grid spacing of 9 km and a temporal resolution of 6 hours. The Global 30 Arc-Second Elevation (GTOPO30) digital elevation
model and the U.S. Geological Survey (USGS) landuse data set were used for D01 and D02, while for D03 and D04, we
used the Advanced Spaceborne Thermal Emission and Reflection Radiometer (ASTER) topography data set (Schmugge et al.,
100 2003) with a horizontal grid spacing of 30 m and the Coordination of Information on the Environment (CORINE) land cover
data provided in 2012 with a horizontal grid spacing of 100 m. A Five- and ten-minute output interval was set for both LES
domains (D03 and D04), respectively. To improve the boundary layer flow, a forest parameterization was implemented in the
model, which will be described in more detail in the following section.

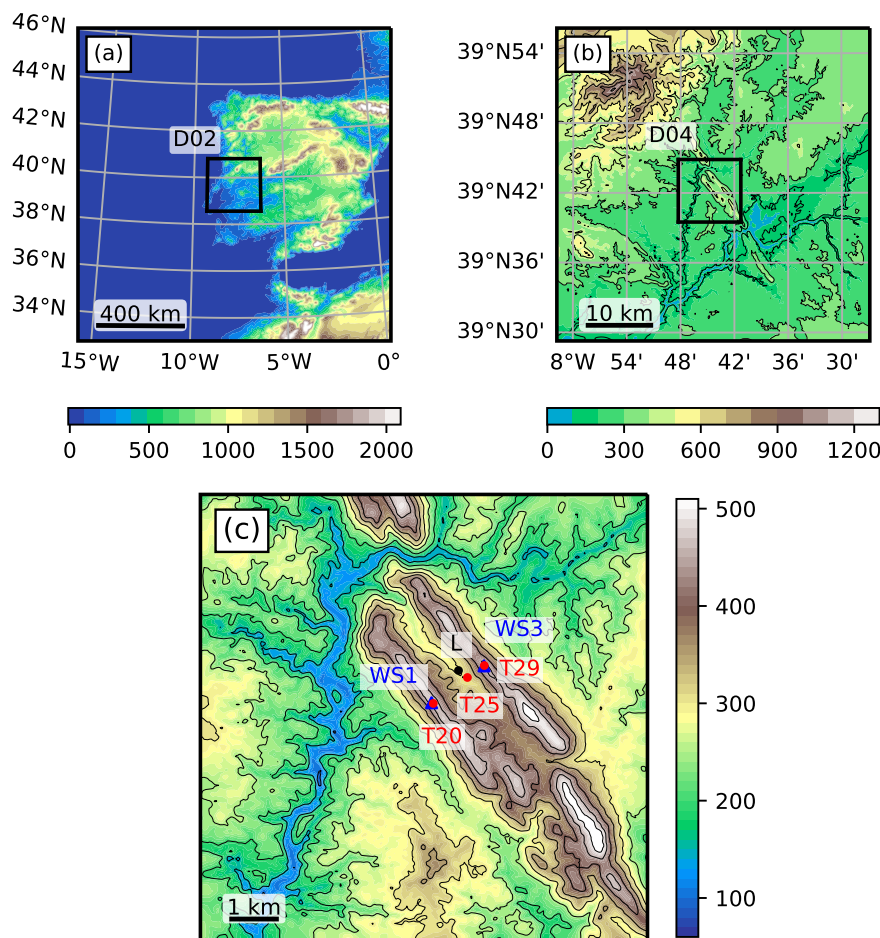


Figure 1. Topographic map of the WRF domains (colour contours). (a) Mesoscale domain D01 using a horizontal grid spacing of 5 km. The extent of D02 is indicated by the black line box. (b) LES Domain D03 using a horizontal grid spacing of 200 m. The extend of D02 is indicated by the black line box. (c) LES Domain D04 using a horizontal grid spacing of 40 m. The locations of the meteorological towers T20, T25 and T29, and the VAD Lidar are marked with dots. The DTU wind scanners WS1 and WS3 are indicated with blue triangles located at the side of towers T20 and T29 (see text for a detailed description). WS2 and WS4 are located at the site of WS1 and WS3 respectively (not shown).

Both LES were run with the forest parametrization (WRF_d03F, WRF_d04F) and without (WRF_d03NF, WRF_d04NF).
105 Both WRF_d03F and WRF_d03NF were run for 49 days and provided the initial and boundary conditions for the innermost domain simulations WRF_d04F and WRF_d04NF. The high-resolution D04 LES WRF_d04F and WRF_d04NF were run for three selected LLJ episodes observed during the IOP Wagner et al. (2019a). Each of the simulations ran for 12 hours starting at 18h UTC on 6, 7 and 22 May 2017.

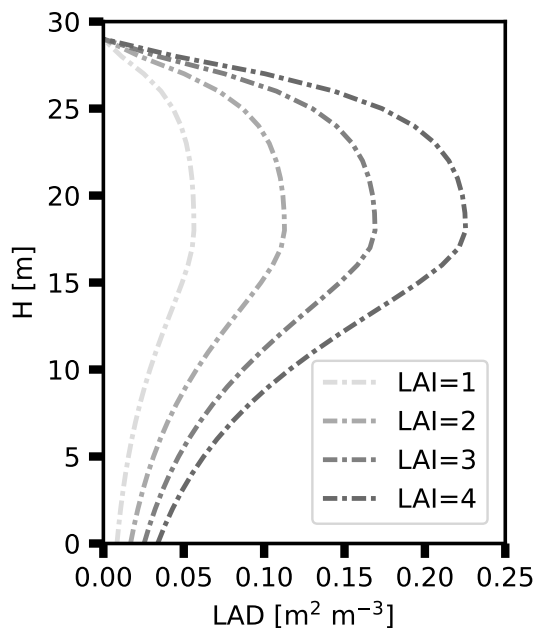


Figure 2. Leaf area density profiles (LAD) for four example values of the leaf area index (LAI) used to parameterize the forest drag. The LAD-profiles represent a pine tree canopy.

2.3 Forest parametrization implementation

110 In the standard WRF-LES model, three-dimensional roughness elements like trees are not explicitly considered and are only
characterized by the roughness length Z_0 (directly obtained from the landuse data set). The explicit treatment of forest drag
in numerical models is of special importance for the realistic development of wind profiles, including inflexion points over
forested areas. In the present work, the forest parameterization following Shaw and Schumann (1992) is implemented in the
WRF model to study its impact on boundary layer flows over forested and complex terrain. The additional forest drag term F_i ,
115 which acts on the lowermost model levels is defined as

$$F_i = -C_d LAD |V| u_i, \quad (1)$$

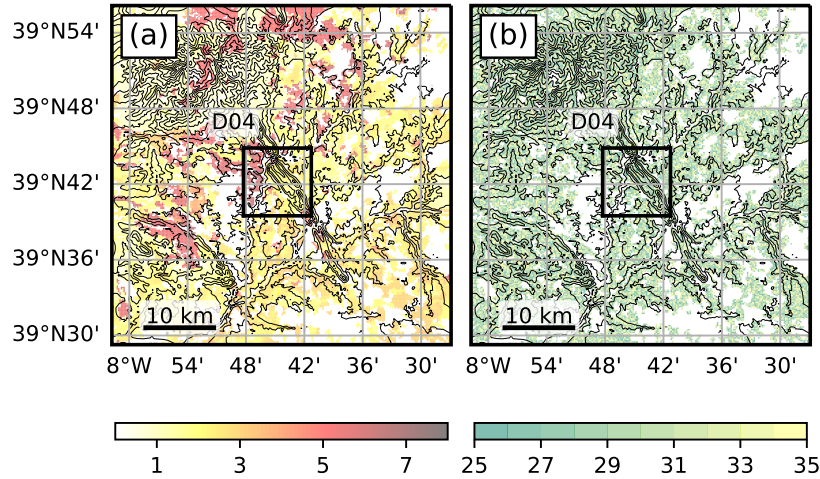


Figure 3. Distribution of (a) leaf area index (LAI) and (b) forest height for domain D03. White areas show regions that are not covered by a forest. The topographical height is indicated with contour lines. The extent of D04 is indicated by the black box.

where $|V|$ is the magnitude of the three dimensional wind vector, u_i is one of the three wind components, $C_d = 0.15$ is a constant drag coefficient, and LAD is the leaf area density profile characterising the trees. The LAD depends on the tree type and the height of the trees. The tree type is defined by means of the leaf area index (LAI). The LAD -profile is computed according to Lalic and Mihailovic (2004) at all grid cells where trees are present as

$$LAD(z) = L_m \left(\frac{h - z_m}{h - z} \right)^n \exp \left[n \left(1 - \frac{h - z_m}{h - z} \right) \right], \quad (2)$$

with

$$n = \begin{cases} 6 & 0 \leq z < z_m \\ 0.5 & z_m \leq z \leq h \end{cases}, \quad (3)$$

where h is the tree height, $L_m = (LAI/h) * 1.69$ is the maximum LAD at height $z_m = 0.6h$ following Mohr et al. (2014). Example LAD -profiles are plotted in Fig. 2 for several LAI using a tree height of 30 m. With increasing LAI , the LAD of the treetop becomes more dominant. The LAI is retrieved from the CORINE landuse data set for the present WRF simulations.

The LAD profile is computed according to equation (2.3) in regions classified as forest. The forest height is an unknown as it is not included in the landuse data. We used a randomly uniformly distributed tree height of $30 \text{ m} \pm 5 \text{ m}$. The tree height used is slightly higher than the trees covering the area, which is about 15 to 20 m, but it ensures that the lowermost two to three model levels remain within the canopy layer. We set the LAD to zero in regions not classified as forest. Figure 3a shows the



135 distribution of the LAI for forested regions in the domain D03 as given by the CORINE data set. Figure 3b shows the randomly distributed forest height. White regions mark areas without forest. In the model, the double ridge is completely covered with trees according to the CORINE dataset, which does not fully match the observed forest distribution in the area during the campaign.

3 Results

140 In the following, we present an evaluation of the WRF-LES simulations (D03 and D04) with/without the forest parametrization in the context of the Perdigo 2017 field campaign. The analysis is divided into two subsections. First, we evaluate the performance of the long-term simulations (D03). Second, a set of low-level jet (LLJ) events is analysed through the short-term simulations (D04) to investigate the impact of the forest parametrization on the LLJ structure over the double ridge.

3.1 Evaluation of the long-term simulations

145 Figure 4 shows the observed and simulated mean diurnal cycle of both the along- and cross-valley wind speeds averaged over the 49-day period covering the IOP for towers T20, T25 and T29. The root mean square error (RMSE) is showed in the bottom panel for each frame. In the observations, the along-valley wind tends to be very weak in the morning hours. In the afternoon, the wind accelerates to a maximum mean of about 2 m s^{-1} at 18h UTC in all three locations. A significant improvement in the along-valley wind speed is visible when the forest parametrization is used (WRF_d03F). At all three towers, the RMSE is typically less than half of its original value for the simulation without the forest parametrization (WRF_d03NF).

150 In the cross-valley direction, the wind observed in the early morning is weak at all three locations. At around 18h UTC, at the crest towers (T20 and T29), the mean cross-valley wind speed reaches its maximum at about 3 m s^{-1} . In the valley bottom, the maximum reaches out about 1.5 m s^{-1} . After the evening transition, the flow slows down, and at midnight it is nearly zero. As noted by Wagner et al. (2019a), the observations showed the presence of a clear daily cycle due to the dominant synoptically calm conditions enhancing the evolution of thermally driven flow systems during the IOP.

155 The cross-valley wind speed in the WRF_d03NF simulation is overestimated throughout the day (see the bottom row in Fig. 4). The introduction of the forest parametrization in the WRF_d03F simulation addresses this problem. However, the effect is too strong, and the wind speed is underestimated at all three towers. In terms of the RMSE, there is no significant difference between the two simulations. Both simulations remain in the range of the standard deviation of observations (shaded areas).

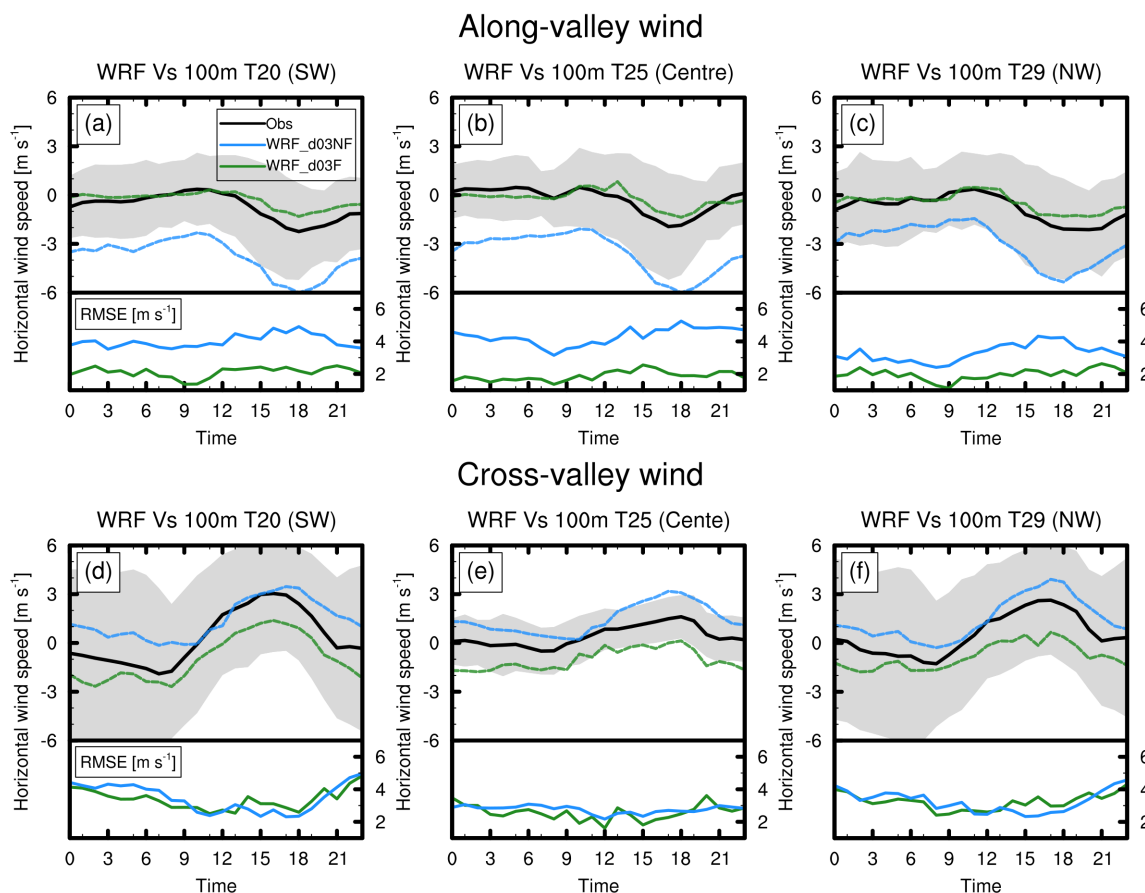


Figure 4. Average diurnal cycle of the along- (upper panels) and cross-valley (bottom panels) wind speed for the 49-day IOP for WRF D03 simulation (left axes) (with and without forest parametrization) and the RMSE for the WRF D03 simulations (right axes) at the three tower locations (T20, T25 and T29, see Fig. 1). The black lines represent values for observations (100 m level), the blue lines represent the simulation WRF_d03NF, and the green lines represent the WRF_d03F. The shaded area corresponds to the standard deviation range from observations.

160 Figure 5 shows the mean diurnal cycle of the wind direction, vector-averaged through the 49-day simulation (and observations) covering the IOP for towers T20, T25 and T29. It should be noted that this is a cyclic measure, both top and bottom ends of the figures represent wind coming from the north. In both crest towers, the wind blows from the north-east in the morning hours. Around noon, it slightly changes the direction to become north-west at the end of the day. In the valley tower (T25), the flow is channelled in the up-valley direction (south-east) through the early morning until 8h UTC. In the following hours, the
165 wind slowly turns to become down-valley (north-west) in the afternoon until late at night (about 22h UTC).

In WRF_d03NF simulation, the model cannot accurately represent the wind direction in the morning hours. The flow is always northwesterly through the day. This issue is corrected in the WRF_d03F simulation, where the flow follows the trend in the observations during the morning and afternoon hours at all three towers.



The underestimation of the wind speed in the cross-valley direction in WRF_d03F simulation may indicate that the use
170 of tree heights of $30 \text{ m} \pm 5 \text{ m}$ is too high, and an improvement in the landuse data with a more realistic LAI and forest
height distribution is necessary. Menke et al. (2020) used data from two pairs of scanning lidars operated in a dual-Doppler
mode during the Perdigão 2017 field campaign to evaluate the performance of WRF-LES along the ridges (using a similar
configuration to WRF_d03F). The results evidence a high sensitivity to the parametrization of surface friction. The model fails
to reproduce the correct signal for the wind amplitude along the ridges both with/without the forest parametrization, although
175 an improvement in the results is observed for the simulation using the forest parametrization. The authors suggested that the
model performance can be improved with a more realistic description of the horizontal distribution of forested areas and tree
heights in the numerical domain.

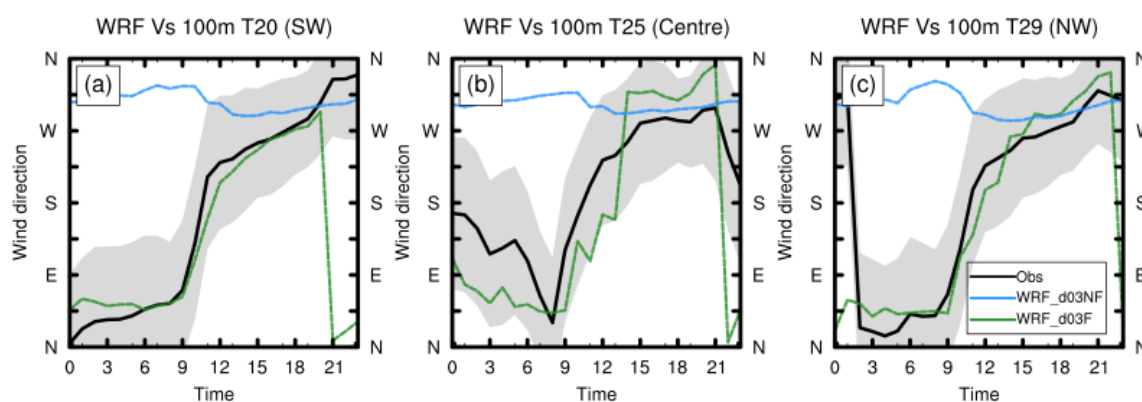


Figure 5. As in Fig 4, but for the diurnal cycle of the vector- averaged wind direction.

3.2 Evaluation short-term simulations

LLJ events, which are mostly a night-time phenomena, are frequently observed above the double ridge. During the IOP, LLJs
180 are mainly the product of thermally driven flows generated by the surrounding mountainous area under synoptically calm
atmospheric conditions. The jets from the northeast occurred more frequently than jets from the southwest (Wagner et al.,
2019a).

Short-term high-resolution numerical simulations with the forest parametrization (WRF_d04F) and without (WRF_d04NF)
are evaluated for three LLJ events observed during the IOP and highlighted in Wagner et al. (2019a). North-east LLJ events
185 during the nights of 7 and 8 May 2017, and a south-west LLJ event on the night of 22 May 2017 are selected to be analysed in
the present work. These events are selected as the jets observed are very stationary.

Panel (a) in figures 6-8 shows lidar composites of the four DTU wind scanners WS1 to WS4 to represent the valley cross-
section horizontal wind structure. Panels (b) to (e) show snapshots of the cross-valley wind speed (colour contours) and poten-
tial temperature of simulations using the forest parametrization (WRF_d03F and WRF_d04F) and without (WRF_d03NF and
190 WRF_d04NF) for the same time as the respective observed cross-valley winds.



The LLJ event on the early morning of 7 May is observed in the Lidar composite (see Fig. 6a). The flow is from the north-east with strong wind speeds (about 5 m s^{-1}) close to the topography and easterly winds above. In the lee of the topography, the signature of internal gravity waves is observed. The horizontal wavelength is similar to that of the valley (about 1.4 km).

Both WRF_d03NF and WRF_d04NF are able to capture the main features of the LLJ episode. The LLJ and the internal gravity wave structure on the lee of the topography is observed in the snapshots of both simulations without using the forest parametrization. However, WRF_d03NF and WRF_d04NF cannot properly represent the south-west flow observed near the ground on the lee of the topography (positive wind in Fig. 6). For WRF_d04NF (see Fig. 6d), the atmosphere on the lee of the topography seems too turbulent, and no clear wind direction is detected.

On the other hand, simulations using the forest parametrization (WRF_d03F and WRF_d04F) better capture the near surface flow. WRF_d03F better represents the atmosphere near the lee slope, but it damps the wave amplitude on the lee side. WRF_d04F seems to better capture the event by conserving the wave structure and showing the near the ground south-west flow. The latter simulation is the one that better represents the LLJ structure when compared to observations.

On the followed day (8 May), another northeasterly LLJ event was observed, but with a southeasterly upper-level wind. The signature of orographically induced gravity waves is visible in the lidar observations near the topography in Fig. 7a. The simulations using the forest parametrization better capture the near the surface atmosphere by reproducing the LLJ and the southeasterly wind between the ground and the LLJ (see Fig. 7c and Fig. 7e). Simulations without the forest parametrization (WRF_d03NF and WRF_d04NF) show a deep LLJ reaching down to the ground on the lee side of the topography, which is not observed in the Lidar data. The forest parametrization seems to correct this issue. Both simulations with the forest parametrization (WRF_d03F and WRF_d04F) better capture the elevated jet and the wave signature in the flow (especially WRF_d04F, see Fig. 7e).

The last LLJ event to be analysed occurred in the early morning of 22 May (see Fig. 8). The event corresponds to a south-westerly LLJ. The LLJ layer is deeper, compared to the other two episodes, at 700 m. Again, the signature of gravity waves can be observed in the lidar data on the lee side of the topography. For this event, all simulations are able to reproduce the main features of the LLJ. The wind direction and magnitude seems to be appropriated in all simulations. However, the forest parametrization in WRF_d04F seems to prevent the LLJ to flow through the slope on the lee side of the topography as observed in the Lidar data. Such feature of the flow was better described in WRF_d04NF, where the LLJ agrees better with the observed LLJ structure in the lee side of the topography.

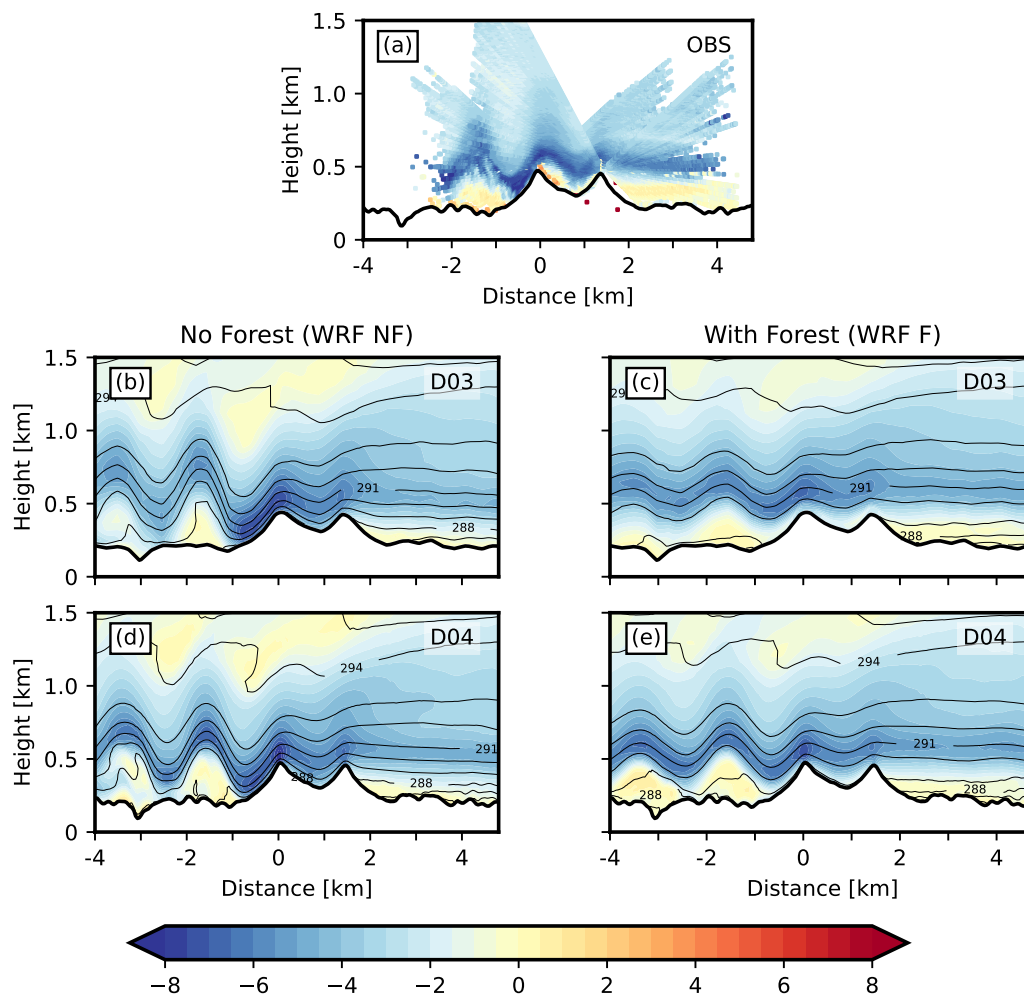


Figure 6. Cross sections of cross-valley wind speed (horizontal wind component across the double ridge) for the Low Level Jet event from NE on 07 May 2017 at 04h00. The x-axis is centred at the location of WS1. Negative velocities indicate flow from NE. (a). Observed winds retrieved from radial velocity composite of DTU Lidars WS1 to WS4. Colour contour interval: 0.5 m s^{-1} . The topography illustrated is identical to that used for D04. (b) – (e) Simulated winds and potential temperature from WRF numerical model. Model data was interpolated to the same cross-section as for observations, which was defined by the location of WS1 and the azimuth scanning angle of 234.68° . WRF simulation without the forest parametrization are displayed in left column, simulation using the forest parametrization are displayed in the right column, for domain D03 (upper row) and D04 (lower row).

In all three LLJ events, the jet structure and the flow close to the surface agrees better with lidar observations when the forest parametrization is switched on (with the exception of the lee slope). Surface winds are reduced, recirculation zones develop and the amplitudes of the gravity waves agree better with lidar observations. A better representation of the surface friction has a significant impact on the formation and wavelength of trapped lee waves (Stiperski and Grubišić, 2011).

220

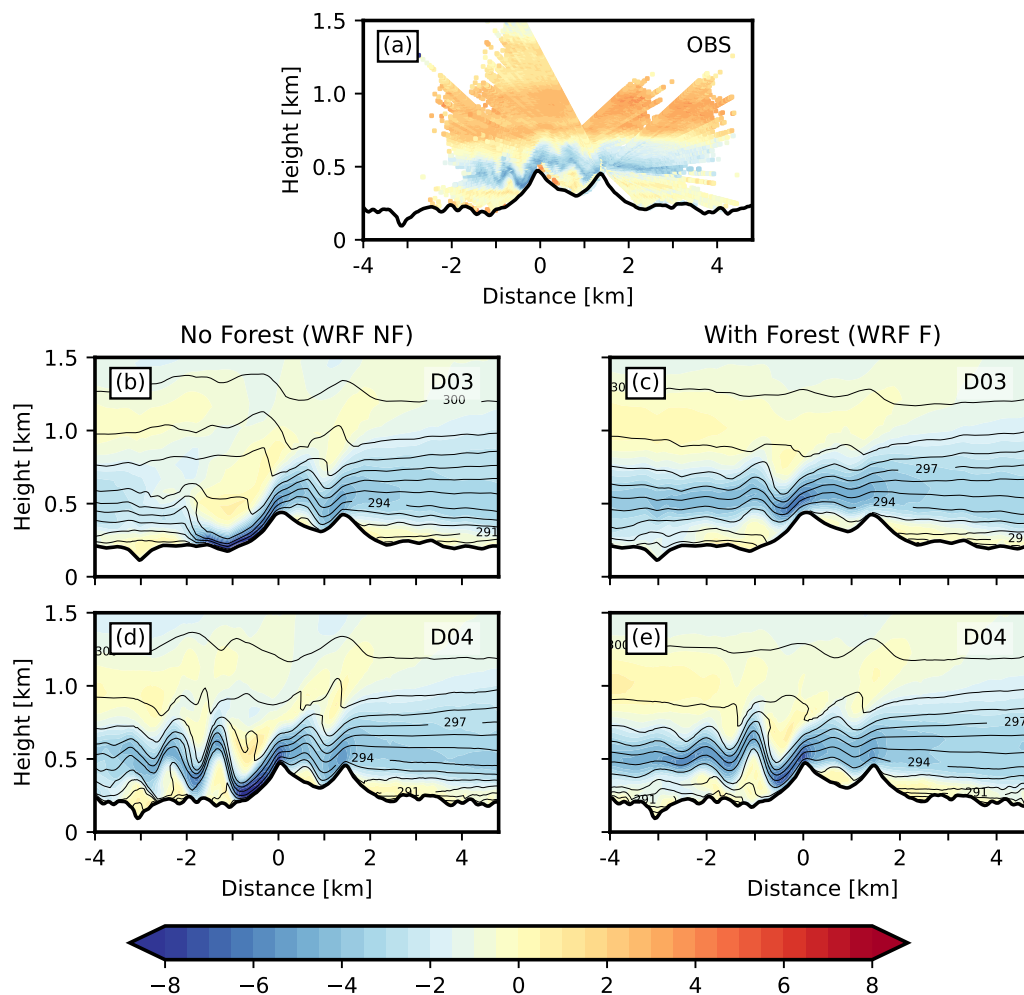


Figure 7. As in Fig. 6, but for Low Level Jet case on 08 May 2017 05:30:00 UTC.

Up to this stage, the evaluation of the high-resolution LES simulations has been carried out for single time snaps to capture the main features of the atmosphere in a cross valley section. In the following, the model performance is evaluated for the period between 7 and 8 May, which comprises the first two LLJ events in a single tower location (T25).

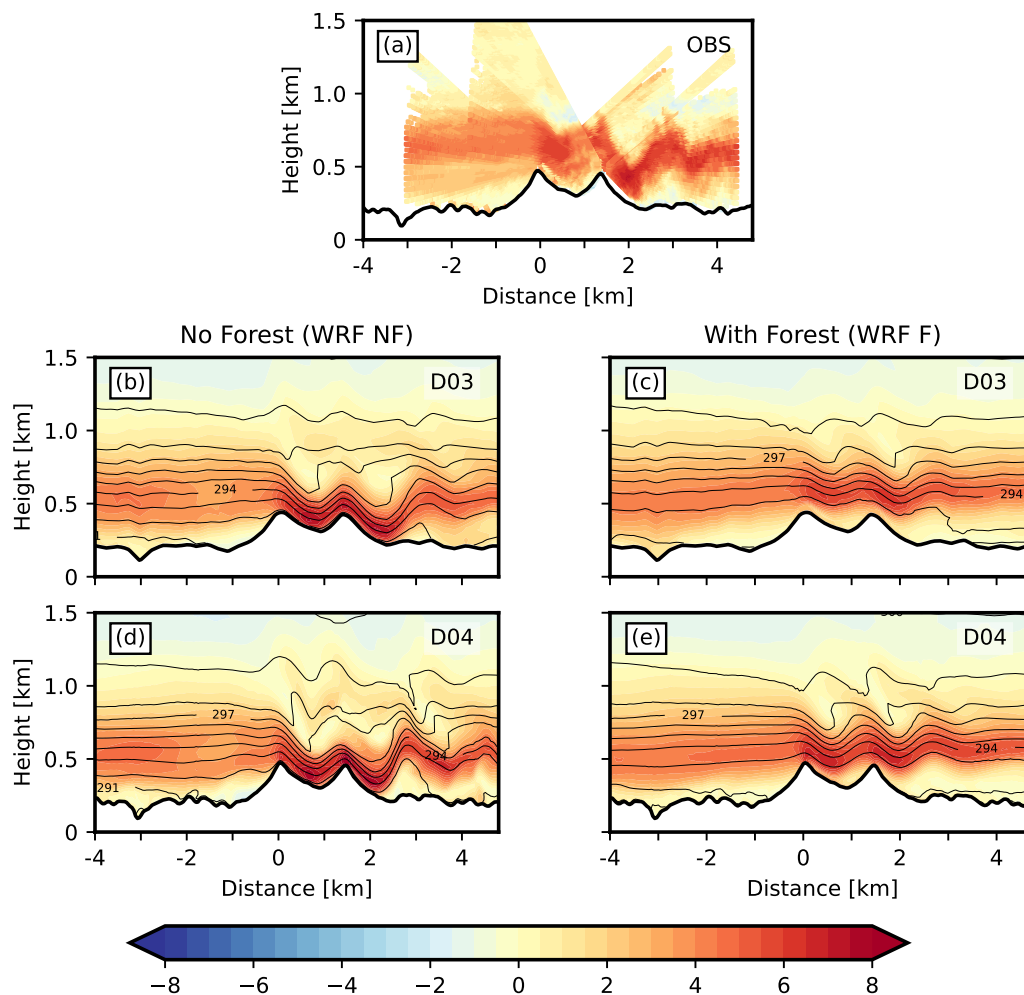


Figure 8. As in Fig. 6, but for Low Level Jet case on 22 May 2017 04:00:00 UTC.

225 Figure 9 shows the time evolution of the wind speed profiles at the valley floor between 00h UTC on 7 May and 06h UTC
 on 8 May for both observations and numerical simulations. Panel (a) presents the data from the tower T25 (20 - 100 m AGL)
 and the VAD wind profiling scans (100 - 1000 m AGL). The instruments are located at 250 m from each other. During the early
 hours of 7 May, the lower atmosphere is characterised by a 100 m deep weak flow layer (below 3 m s^{-1}). The LLJ signature
 is observed aloft reaching wind speeds of about 8 m s^{-1} between 02h UTC and 06h UTC. After 06h UTC, the ground layer
 230 starts to grow to a depth of 200 m at 09h UTC. During midday and afternoon, the whole atmosphere becomes turbulent, and a
 convective scenario is observed until 18h UTC when the turbulence begins to vanish.

In the early hours of 8 May, the atmosphere becomes quiet again, and the LLJ is hardly visible. The weak flow layer close
 to the ground is deeper than the day before (as deep as 200 m), and the wind close to the surface remains weak. At 03h UTC
 the flow layer starts to deepen, reaching 500 m at 6h UTC while maintaining the magnitude of the wind speed.



235 Panels (b) and (c) in the Fig. 9 presents the results for WRF_d04F and WRF_d04NF respectively at the location of the tower
T25. Both simulations ran for 12 hours between 18h and 06h UTC for 6 and 7 May. The simulations capture the main features
observed in the tower and Lidar data. However, important differences can be noted. The LLJ event observed in the early
morning of 7 May is reproduced by both simulations, but weaker than observed. WRF_d04NF fails to correctly reproduce the
layer of weak flow close to the ground. This issue is addressed by WRF_d04F. The introduction of the forest parametrization
240 helps in slowing down the wind close to the ground. Thus improving the representation of the near surface winds.

In the second simulation period (18h - 06h UTC for 7 May), both simulations overestimate the magnitude of the LLJ.
WRF_d04NF better represents the near-surface flow layer than the previous night, but again, WRF_d04F better captures the
weak character of such a layer. The growth of the flow layer at 03h UTC is well reproduced in both simulations.

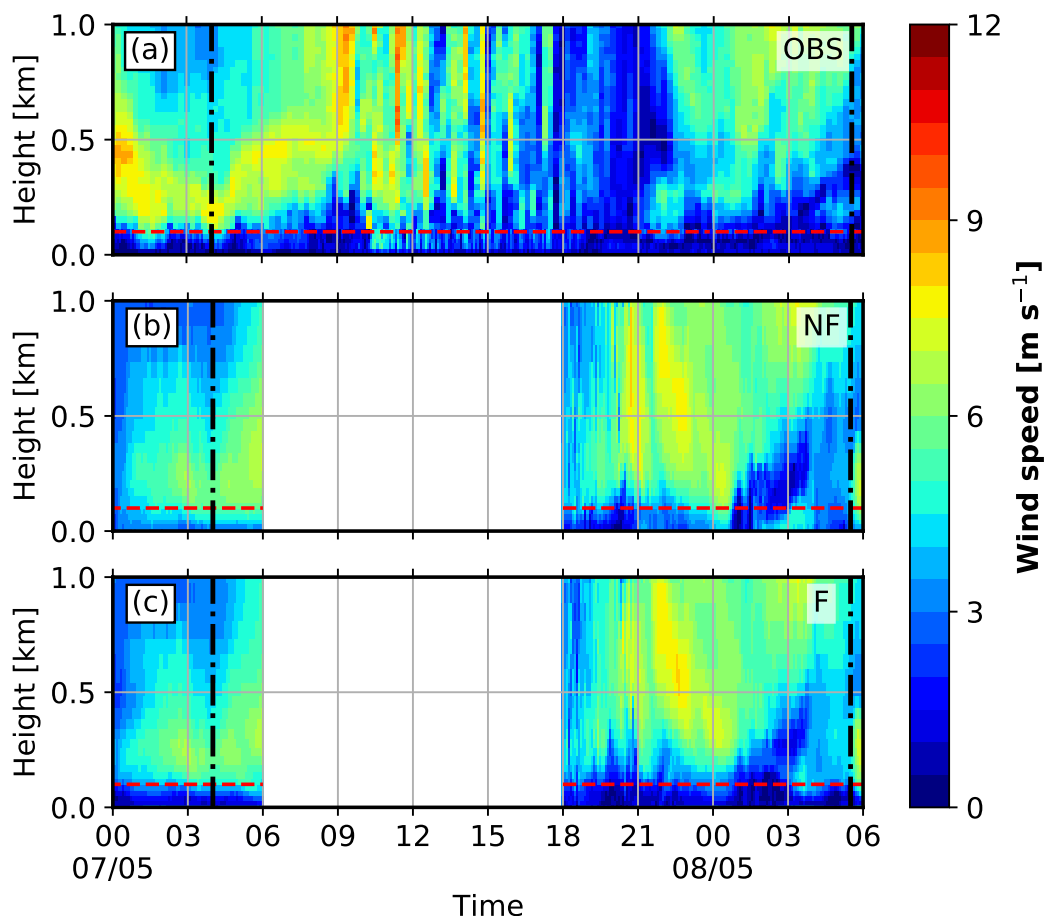


Figure 9. Vertical structure of the horizontal wind speed from observations using data from the tower T25 up to 100 m, and the University of Oklahoma’s VAD wind profiling scans from 100 m up to 1000 m (a). Simulation without the forest parametrization (WRF_d04NF) (b) and with the forest parametrization (WRF_d04F) (c). The results for the WRF simulations have been taken at the location where the University of Oklahoma’s wind profiler scan was located during the field campaign (see fig. 1c). Red dashed line in the plots represent the 100 m above ground height. Dash-dotted vertical black line represents the time at which LLJ events are observed (see text for reference).

To quantify the impact of the forest parametrization on the wind profile, the RMSE and the bias are calculated at the T25 tower location. The calculation is based on the two simulated periods; between 7 May at 00h to 06h and 7 May at 18h to 8 May at 06h UTC. Figure 10 shows the results for both WRF_d04NF and WRF_d04F simulations.

The influence of the forest parametrization in the first 100 m AGL is important. The effect is the largest immediately near the surface, where WRF_d04F presents 1.5 m s^{-1} difference to WRF_d04NF in terms of the RMSE (see Fig. 10a). The effect of the parametrization vanishes with height, however, its effect can be observed up to 500 m AGL.

As for the bias, a similar behaviour as for the RMSE is found (see Fig. 10b). WRF_d04F improves the model performance in the first metres above the ground. It is worth noting that the model always presents an overestimation of the wind speed



through the first 1000 m AGL. The forest parametrization adds drag which helps to slow down the wind near the ground, such an effect is positively quantified in the improvement of the error.

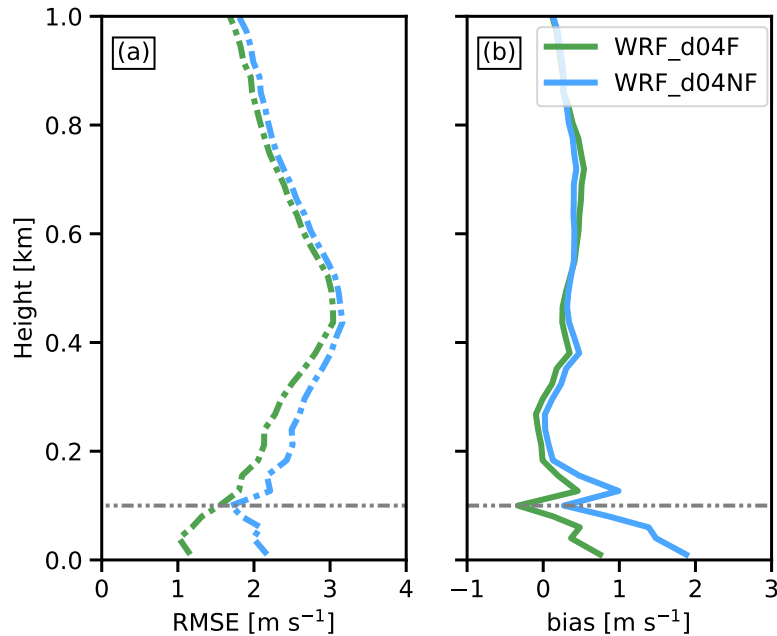


Figure 10. Vertical profiles of the root-mean-squared-error (RMSE, (a) and bias (b) of wind speed with respect to observations for WRF_d04NF (blue lines), and WRF_d04F (green lines). From the ground up to 100m, data from the tower T25 is used, while from 100 m to 1000m data from the University of Oklahoma’s VAD wind profiling scans is used. The grey dashed line marks the 100 m level. The results are computed between 7 May 00h UTC - 7 May 06h UTC and 7 May 18h - 8 May 06h UTC.

Figure 11 shows the evolution of the wind direction at tower T25 location for both the observations and the numerical
255 simulations. Observations show an upper level wind from the southeast through the whole period. The LLJ event observed in the early morning of 7 May corresponds to a northeasterly cross-valley wind. Near the ground, a wind from the north/northeast dominates (cross-valley). During the day hours, the up-valley wind (southeast) dominates the atmosphere with some burst of north/south winds. During the following night, the up-valley wind (southeast) near the ground does not change direction and remains up-valley until the end of the period at 06h UTC. Immediately above the near-surface flow layer, a cross-valley wind
260 (north-east) is observed, which may be interpreted as the signature of the LLJ.

Both WRF_d04NF and WRF_d04F simulations capture the main features of the flow. A northeasterly wind is simulated at 100 m AGL, and the upper-level wind from the southeast is well simulated in both periods as well. However, WRF_d04NF cannot represent the near-surface wind. A constant up-valley wind was observed through out the period, which is not represented in the WRF_d04NF.

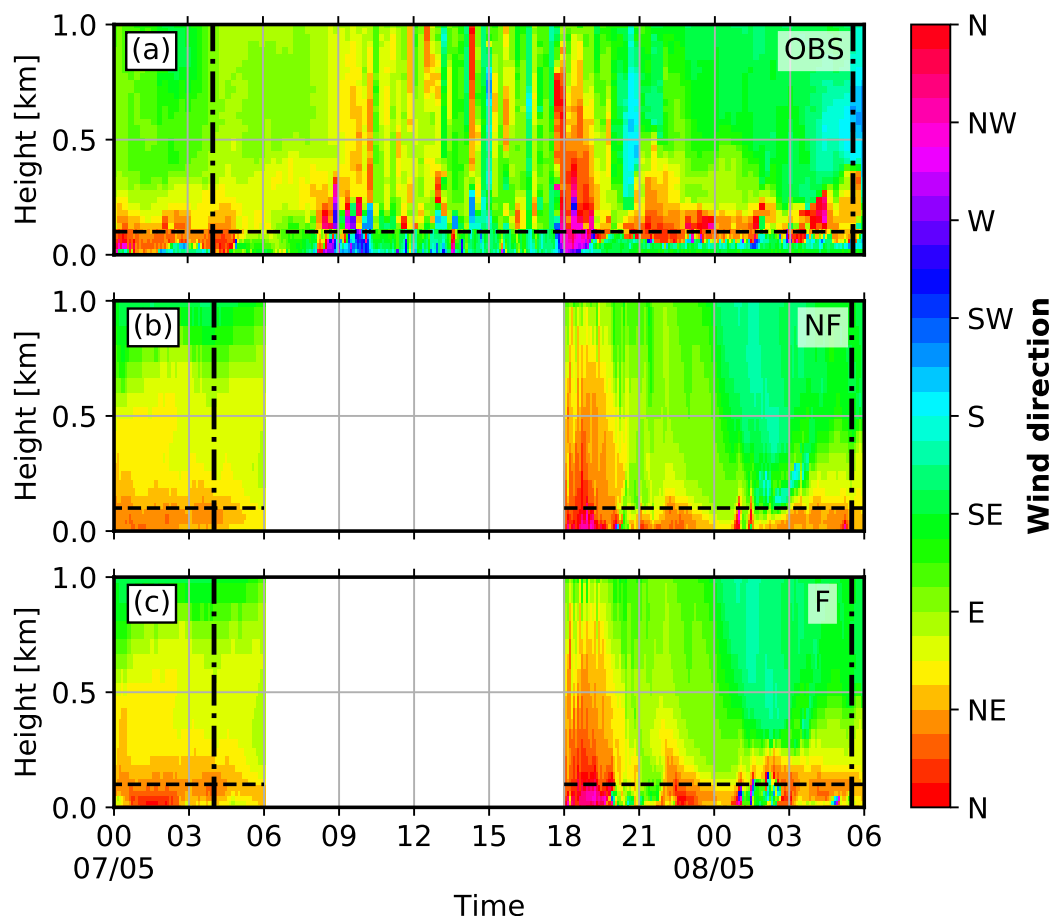


Figure 11. As in Fig. 9, but for the wind direction.

265 The simulation WRF_d04F (see Fig. 11c) better represents the wind direction of the near-surface flow in the early morning on 7 May. A clear wind from the north is displayed in the first few hours of observation, which later vanishes to become southeast at about 6h00. The model cannot reproduce the constant up-valley wind (southeastern wind) observed near the ground for the second period. However, WRF_d04F was able to reproduce the up-valley wind for short periods.

It is worth noting that the wind speed near the surface is very weak (below 3 m s^{-1}), which makes the task to capture
270 the proper wind direction challenging. Above the near-surface flow layer, where the wind is stronger, the model displays a better performance. Since at low wind speeds wind direction fluctuations are important, statistics of this quantity have not been calculated due to the possible large RMSE values that may lead to misinterpretation of the results (Chow et al., 2006).



4 Conclusions

The performance of LES simulations using the Weather Research and Forecasting (WRF-V4.0.1) model (Skamarock et al.,
275 2019) with/without the implementation of a forest parametrization has been tested in the context of the Perdigão 2017 field
campaign (Fernando et al., 2019). A similar configuration to that presented in Wagner et al. (2019a) is used with the addition
of a subsequent inner domain with a horizontal grid spacing of 40 m. Results are validated and tested against observational
data retrieved during the campaign's intensive observational period (IOP) between April and June 2017.

Long-term simulations (49-day) covering the IOP were conducted using a horizontal grid spacing of 200 m. The mean
280 diurnal cycle during the IOP shows a significant improvement of the along-valley wind speed and wind direction when using
the forest parametrization (WRF_d03F). However, the drag imposed by the parametrization generates an underestimation of
the cross-valley wind speed. This may indicate that the use of tree heights of $30 \text{ m} \pm 5 \text{ m}$ is too high, and an improvement in
the landuse data with a more realistic leaf area index (LAI) and forest height distribution is necessary.

Low-level jets (LLJ) events, which are mostly night-time phenomena, are frequently observed above the double ridge (Wag-
285 ner et al., 2019a). Short-term high-resolution numerical simulations, using a 40 m horizontal grid spacing, with the forest
parametrization (WRF_d04F) and without (WRF_d04NF) are evaluated for three LLJ events observed during the IOP.

The simulations using the forest parametrization better capture the main features of the observed LLJ than the simulations
without it. The additional drag from the forest parametrization helps to better reproduce the near-surface flow structure with
re-circulation zones near the slopes that agree better with the Lidar observations.

290 The model performance is further evaluated for the period comprising the first two LLJ events for the valley tower site (T25).
The forest parametrization systematically improves the representation of the wind near the surface, both the wind magnitude
and the wind direction, throughout the LLJ events. Although the parametrization is only applied to the first three model levels
(about 30 m AGL), its positive impact is visible up to a height of 500 m above the ground, in terms of a reduced RMSE and
bias.

295 The results presented show that the addition of a forest parametrization can positively influences the simulation of the winds
in the boundary layer over moderate complex terrain. Further improvement might be achieved with the use of more accurate
landuse data with a more realistic LAI and forest height distribution. The investigation of the benefit of a forest parametrization
for other atmospheric conditions and different locations is left for a future work.

Code and data availability. The WRF source code is available at: <http://www2.mmm.ucar.edu/wrf/users/>. The model output to produce the
300 figures displayed in the present work, along with the WRF namelist to perform the numerical simulations are openly available in Zenodo at
Quimbayo-Duarte et al. (2021). The observational data used in this work can be openly found in Zenodo at Quimbayo-Duarte et al. (2021).
The full field experiment dataset can be found in the official Perdigão 2017 field campaign repository at (re3data.org, 2019)



305 *Author contributions.* Julian Quimbayo-Duarte performed the model evaluation and wrote the manuscript. Johannes Wagner performed the WRF simulations, implemented the forest parameterization in the model and helped in the data post-processing. Norman Wildmann conducted lidar observations during the Perdigão campaign provided lidar data and helped to analyse observation data. Thomas Gerz took part in the Perdigão campaign and assisted in analysing the results. Juerg Schmidli assisted in analysing the results and manuscript writing. All authors contributed to the paper by discussing the results and by proofreading the manuscript.

Competing interests. All authors declare to have no competing interests.

310 *Acknowledgements.* We thank José Palma, University of Porto, José Carlos Matos and the INEGI team, as well as the research groups from DTU and NCAR for the successful collaboration and realization of the Perdigão campaign. Additionally, we thank the municipalities of Alvaiade and Vila Velha de Rodão in Portugal for local support. Thanks a lot to R. Menke and J. Mann from DTU for providing the wind scanner data and to NCAR EOL for the tower data.



References

- 315 Aumond, P., Masson, V., Lac, C., Gauvreau, B., Dupont, S., and Berengier, M.: Including the drag effects of canopies: real case large-eddy simulation studies, *Boundary-layer meteorology*, 146, 65–80, 2013.
- Chow, F. K., Weigel, A. P., Street, R. L., Rotach, M. W., and Xue, M.: High-resolution large-eddy simulations of flow in a steep Alpine valley. Part I: Methodology, verification, and sensitivity experiments, *Journal of Applied Meteorology and Climatology*, 45, 63–86, 2006.
- Dupont, S. and Brunet, Y.: Impact of forest edge shape on tree stability: a large-eddy simulation study, *Forestry*, 81, 299–315, 2008.
- 320 Dupont, S., Brunet, Y., and Finnigan, J. J.: Large-eddy simulation of turbulent flow over a forested hill: Validation and coherent structure identification, *Quarterly Journal of the Royal Meteorological Society*, 134, 1911–1929, 2008.
- Fernando, H., Mann, J., Palma, J., Lundquist, J. K., Barthelmie, R. J., Belo-Pereira, M., Brown, W., Chow, F., Gerz, T., Hocut, C., et al.: The Perdigao: Peering into microscale details of mountain winds, *Bulletin of the American Meteorological Society*, 100, 799–819, 2019.
- Hong, S.-Y. and Kim, S.-W.: Stable boundary layer mixing in a vertical diffusion scheme, in: 18th Symposium on Boundary Layers and
325 Turbulence B, vol. 16, 2008.
- Lalic, B. and Mihailovic, D. T.: An empirical relation describing leaf-area density inside the forest for environmental modeling, *Journal of Applied Meteorology*, 43, 641–645, 2004.
- Liu, Z., Ishihara, T., He, X., and Niu, H.: LES study on the turbulent flow fields over complex terrain covered by vegetation canopy, *Journal of Wind Engineering and Industrial Aerodynamics*, 155, 60–73, 2016.
- 330 Mann, J., Angelou, N., Arnqvist, J., Callies, D., Cantero, E., Arroyo, R. C., Courtney, M., Cuxart, J., Dellwik, E., Gottschall, J., et al.: Complex terrain experiments in the new european wind atlas, *Philosophical Transactions of the Royal Society A: Mathematical, Physical and Engineering Sciences*, 375, 20160 101, 2017.
- Mazoyer, M., Lac, C., Thouron, O., Bergot, T., Masson, V., and Musson-Genon, L.: Large eddy simulation of radiation fog: impact of dynamics on the fog life cycle, *Atmospheric Chemistry and Physics*, 17, 13 017–13 035, 2017.
- 335 Mellor, G. L. and Yamada, T.: Development of a turbulence closure model for geophysical fluid problems, *Reviews of Geophysics*, 20, 851–875, 1982.
- Menke, R., Vasiljević, N., Mann, J., and Lundquist, J. K.: Characterization of flow recirculation zones at the Perdigão site using multi-lidar measurements, *Atmospheric Chemistry and Physics*, 19, 2713–2723, 2019.
- Menke, R., Vasiljević, N., Wagner, J., Oncley, S. P., and Mann, J.: Multi-lidar wind resource mapping in complex terrain, *Wind Energy
340 Science*, 5, 1059–1073, 2020.
- Mohr, M., Jayawardena, W., Arnqvist, J., and Bergström, H.: Wind energy estimation over forest canopies using WRF model, *European Wind Energy Association, EWEA*, 2014.
- Quimbayo-Duarte, J., Wagner, J., Wildmann, N., Gerz, T., and Schmidli, J.: Data accompanying the paper titled: Evaluation of a forest parameterization to improve boundary layer flow simulations over complex terrain., <https://doi.org/10.5281/zenodo.5566933>, 2021.
- 345 re3data.org: Perdigao Field Experiment; editing status 2020-03-20; re3data.org - Registry of Research Data Repositories, <http://doi.org/10.17616/R31NJMN4>, 2019.
- Schmugge, T. J., Abrams, M. J., Kahle, A. B., Yamaguchi, Y., and Fujisada, H.: Advanced spaceborne thermal emission and reflection radiometer (ASTER), in: *Remote Sensing for Agriculture, Ecosystems, and Hydrology IV*, vol. 4879, pp. 1–12, International Society for Optics and Photonics, 2003.



- 350 Shaw, R. H. and Schumann, U.: Large-eddy simulation of turbulent flow above and within a forest, *Boundary-Layer Meteorology*, 61, 47–64, 1992.
- Skamarock, W. C., Klemp, J. B., Dudhia, J., Gill, D. O., Liu, Z., Berner, J., Wang, W., Powers, J. G., Duda, M. G., Barker, D. M., et al.: A description of the advanced research WRF model version 4, National Center for Atmospheric Research: Boulder, CO, USA, p. 145, 2019.
- 355 Stiperski, I. and Grubišić, V.: Trapped lee wave interference in the presence of surface friction, *Journal of the atmospheric sciences*, 68, 918–936, 2011.
- Wagner, J., Gerz, T., Wildmann, N., and Gramitzky, K.: Long-term simulation of the boundary layer flow over the double-ridge site during the Perdigão 2017 field campaign, *Atmospheric Chemistry and Physics*, 19, 1129–1146, 2019a.
- Wagner, J., Wildmann, N., and Gerz, T.: Improving boundary layer flow simulations over complex terrain by applying a forest parameterization in WRF, *Wind Energy Science Discussions*, 2019, 1–25, <https://doi.org/10.5194/wes-2019-77>, 2019b.
- 360 Wagner, T. J., Klein, P. M., and Turner, D. D.: A new generation of ground-based mobile platforms for active and passive profiling of the boundary layer, *Bulletin of the American Meteorological Society*, 100, 137–153, 2019c.
- Zaïdi, H., Dupont, E., Milliez, M., Musson-Genon, L., and Carissimo, B.: Numerical simulations of the microscale heterogeneities of turbulence observed on a complex site, *Boundary-layer meteorology*, 147, 237–259, 2013.